

---

# FED-CD: FEDERATED CAUSAL DISCOVERY FROM INTERVENTIONAL AND OBSERVATIONAL DATA

---

A PREPRINT

**Amin Abyaneh**

McGill University, Montreal, Canada

amin.soleimaniabyaneh@mail.mcgill.ca

**Nino Scherrer**

ETH Zürich, Zürich, Switzerland

nino.scherrer@gmail.com

**Patrick Schwab**

GlaxoSmithKline, Artificial Intelligence  
and Machine Learning  
Zug, Switzerland  
patrick.x.schwab@gsk.com

**Stefan Bauer**

KTH Royal Institute of Technology &  
CIFAR Azrieli Global Scholar  
Tübingen, Germany  
stefan.bauer@tuebingen.mpg.de

**Bernhard Schölkopf**

Max Planck Institute for Intelligent Systems  
Tübingen, Germany  
bs@tuebingen.mpg.de

**Arash Mehrjou**

GlaxoSmithKline, Artificial Intelligence  
and Machine Learning &  
Max Planck Institute for Intelligent Systems  
Tübingen, Germany &  
ETH Zürich, Zürich, Switzerland  
amehrjou@ethz.ch

June 27, 2023

## ABSTRACT

Existing causal discovery methods typically require the data to be available in a centralized location. However, many practical domains, such as healthcare, limit access to the data gathered by local entities, primarily for privacy and regulatory constraints. To address this, we propose FED-CD, a federated framework for inferring causal structures from distributed datasets containing observational and interventional data. By exchanging updates instead of data samples, FED-CD ensures privacy while enabling decentralized discovery of the underlying directed acyclic graph (DAG). We accommodate scenarios with shared or disjoint intervened covariates, and mitigate the adverse effects of interventional data heterogeneity. We provide empirical evidence for the performance and scalability of FED-CD for decentralized causal discovery using synthetic and real-world DAGs.

**Keywords** Causal Discovery, Federated Learning, Decentralized Data, Bayesian Networks

## 1 Introduction

The fundamental and often challenging problem of discovering cause-effect relationships has long captivated the attention of statisticians [Pearl, 2009], and other disciplines such as epidemiology [Vandenbroucke et al., 2016] and computational biology [Sachs et al., 2005]. Inferring causal relationships is critical for understanding the underlying mechanisms behind random variables, and predicting the effect of externally imposed manipulations on causal dynamics of systems [Spirtes, 2010]. Conventional approaches to causal discovery primarily rely on centralized data. However, when dealing with sensitive information like patients' medical records, preserving privacy is essential and protected by strict regulations. As a result, institutions often refrain from disclosing sensitive data required to infer causal structures. Privacy concerns extend beyond the medical domain, arising in economics, biology, and engineering [Glancy, 2012, Papernot et al., 2016].

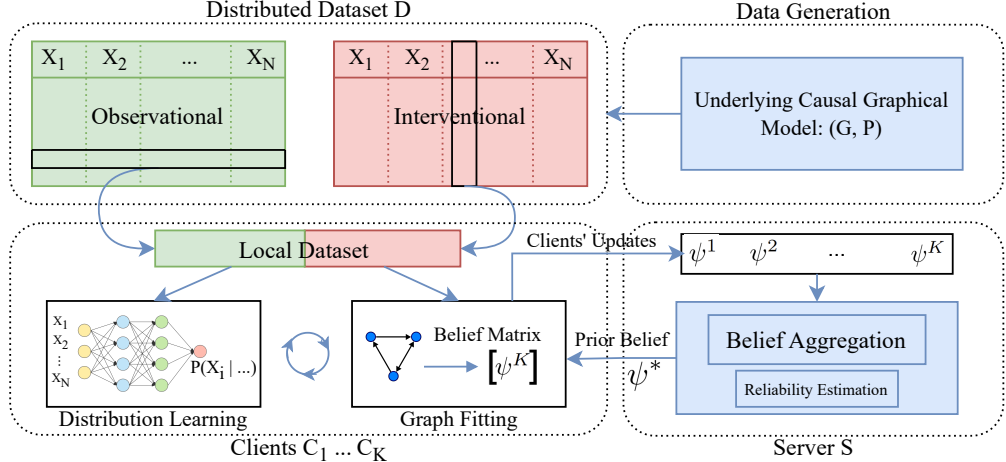


Figure 1: Overview of FED-CD and its federated setup. We only represent a single client, as the rest perform similar operations in parallel.

Consequently, researchers have turned to privacy-preserving causal discovery to leverage decentralize data. Most notably, federated learning [Li et al., 2020] is employed to learn causal structures while avoiding privacy violations. Yet, previous efforts tend to suffer from limitations. For instance, DARLS framework [Ye et al., 2022] is limited to data generated from a linear underlying causal mechanism, whereas DS-FCD [Gao et al., 2021] offers no priority to clients with more valuable contributions. Critically, previous attempts solely utilize observational data gathered from unperturbed systems, which restricts the discovered structures to Markov equivalence classes [Yang et al., 2018, Spirtes and Zhang, 2016]. Gathering interventional data by applying controlled perturbations alleviates such shortcomings through improving identifiability [Yang et al., 2018, Ke et al., 2019].

We propose FED-CD, a federated approach for causal discovery from decentralized observational and interventional data. We learn a global causal structure from a federation of clients, without direct access to each client’s local data. To this end, clients adopt a neural causal discovery method, for instance Lippe et al. [2021], to discover a local structure from their private data. These local findings are then aggregated on a server while adhering to two important criteria. Firstly, clients with more reliable knowledge about intervened variables have a larger impact on the discovery process. And secondly, no data samples are communicated between the clients, or to the server, since only probabilistic updates are exploited in the aggregation process.

Conforming to the mentioned criteria, FED-CD can confidentially aggregate clients’ updates based on the reliability of their local dataset. Clients’ contributions are rated by the extent of their access to interventional data and the location of interventions in the overall causal structure, owing to our novel knowledge aggregation method. Therefore, a client presents a stronger vote on the existence of a cause-effect relationship in the vicinity of its interventional data. Moreover, our approach poses few restrictive assumptions about the data generation mechanism, and endures a level of heterogeneity in interventional data. We empirically demonstrate that FED-CD performs similar to the centralized approaches, without directly sharing clients’ private data, for synthetic and real-world causal structures. An overview of FED-CD is presented in Figure 1.

## 2 Related Work

Attempts to discover causal structures from distributed data were already in effect before the rise of federated learning. For instance, Gou et al. [2007] proposes a two-step approach: they obtain a local Bayesian network for each partition of the dataset and then, utilizing conditional independence tests, they combine local DAGs into a final global model. Moreover, in Na and Yang [2010], the authors propose a voting-based approach that accounts for sending local models to a central site where the final structure is determined by looking for frequently occurring parts among the local DAGs. Both these methods operate for only a single round; thus, no iterative improvement happens, and the discovered DAG is decided by the majority of the clients.

There has been a surge in research at the intersection of causal discovery and federated learning. Among these, DS-FCD [Gao et al., 2021] is a gradient-based method where at each round, clients learn an adjacency matrix to approximate

the causal graph and neural network representation to approximate the causal mechanisms based on their local data. Another related work is developed by Ng and Zhang [2021], where they convert a centralized optimization problem – earlier proposed by Zheng et al. [2018] – to a distributed one and solve it through inter-client collaboration. DARLS [Ye et al., 2022] is another method that counts on generalized linear models and distributed optimization to find an optimal DAG without violating clients’ privacy. Authors in Mian et al. [2023] enhance the previous work by avoiding the exchange of model parameters. Yet, generally, federated causal discovery methods are either limited to linear causal mechanisms, or only consider homogeneous data. Moreover, the rich information provided by interventional data is not exploited in any federated work to the best of our knowledge.

Finally, due to relevancy to our topic, we present the background of continuous optimization-based causal discovery methods. Unlike score-based methods, this class of algorithms avoids the combinatorial greedy search over DAGs by employing gradient-based approaches. DAGs with NO TEARS [Zheng et al., 2018] is considered the first to reformulate graph search problem as a continuous optimization problem [Vowels et al., 2021]. DAG-GNN [Yu et al., 2019] extends NO TEARS by incorporating deep learning to capture complex nonlinear mappings, by proposing a deep generative model and applying a variant of the structural constraint to learn the underlying DAG.

When it comes to neural causal discovery methods, SDI [Ke et al., 2019] and DCDI [Brouillard et al., 2020], are known to discover causal DAG leveraging the combination of observational and interventional data for discrete and continuous data, respectively. Other approaches within this context, such as SAM [Kalainathan et al., 2018] only consider observational data. ENCO [Lippe et al., 2021] presents an efficient DAG discovery method for directed, acyclic causal graphs utilizing both observational and interventional data. They present the graph search as optimization of independent edge likelihoods, and reliably recover DAGs for large feature spaces.

### 3 Problem Setup and assumptions

*Causal graphical models* (CGM) provide mathematical abstraction to quantitatively describe causal relations between random variables. A CBN is a pair  $(G, P)$ , where  $G = (X, E)$  is a *directed acyclic graph* (DAG), and  $P$  is a distribution faithful to  $G$  [Spirtes, 2010]. Within  $G$ , each node,  $X_i \in X \forall i \in \{1, \dots, N\}$ , represents a random variable, and a directed edge  $X_i \rightarrow X_j$  denotes the existence of a cause-effect relationship from  $X_i$  to  $X_j$  [Pearl, 2009]. We denote the binary adjacency matrix of  $G$  by  $\text{adj}(G)_{N \times N}$ , and assume causal sufficiency of the CGM, i.e., all common causes of variables are included and observable.

An *intervention* on a random variable  $X$  is an applied perturbation on the system, such that it overrides the natural values of  $X$  that affects its probability distribution and (possibly) alters the DAG. We call the gathered data from an unperturbed system *observational*,  $D_{\mathcal{O}}$ , and we use the term *interventional*,  $D_{\mathcal{I}}$ , when the data is gathered from the perturbed system. The collection of these two datasets is denoted by  $D := \{D_{\mathcal{O}}, D_{\mathcal{I}}\}$ , that is a centralized dataset generated by perturbed and unperturbed causal mechanisms described by  $(G, P)$ . Moreover, interventions within  $D_{\mathcal{I}}$  are perfect,  $p_{\mathcal{I}}(X_i \mid \text{Pa}(X_i)) = p_{\mathcal{I}}(X_i)$ , where  $p_{\mathcal{I}}$  is the distribution of intervened  $X_i$ .

Our proposed federated setup consists of a central node acting as a server and  $K$  other nodes as clients. We denote the server with  $S$  and the clients with,  $C_k \forall k \in \{1, \dots, K\}$ . Each client is an independent processing unit, and can only communicate with the server. The centralized dataset  $D$  is distributed among the clients, where each client  $C_k$  has access to a (not necessarily disjoint) subset of  $D$ , called  $D^k := \{D_{\mathcal{O}}^k, D_{\mathcal{I}}^k\}$ . To utilize the entire dataset for structure discovery, we assume these subsets to span the entire  $D$ , such that  $D = \bigcup_{k=1}^K D^k$ .

Any dataset can be distributed either horizontally or vertically. Horizontal distribution leads to clients having access to the entire set of features, but only a fraction of samples. A vertical split, however, provides access to only a subset of features in the original centralized data. We consider a horizontal split for  $D_{\mathcal{O}}$  and different setups with either vertical or horizontal distribution of  $D_{\mathcal{I}}$ . Therefore, we assume that clients are aware of all the dataset features, but might not have access to interventional data corresponding to each random variable,  $X_i$ . The accessible set of intervened variables for each client  $C_k$  is represented by  $X_{\mathcal{I}}^k \subset X$ .

**Problem statement** Within the described federated setting, we focus on recovering the DAG,  $G$ , rather than the underlying probability distribution,  $P$ . We enforce a strict restriction on direct exchange of  $D^k$  samples either between two arbitrary clients,  $C_i$  and  $C_j$ , or to the server,  $S$ .

### 4 Federated Causal Discovery From Decentralized Data

Following the federated learning paradigm, clients participating in FED-CD collaborate through an iterative discovery process. Each federated round fundamentally consists of two stages:

1. Local discovery (Section 4.1): Each client applies a local causal discovery method (LCDM) to yield a *prior belief* about  $G$  while considering existing belief from previous rounds. Therefore, a client,  $C_k$ , can securely share its knowledge of the causal structure with the server, without disclosing samples or model parameters.
2. Global aggregation (Section 4.3): The server employs an aggregation method to find the updated belief from a collection of clients' communicated beliefs. Then, the server broadcasts the *aggregated belief* back to all clients, which they utilize for local discovery in the next round.

We start with the first step in Section 4.1 by discussing the nature of the prior belief knowledge and LCDMs. Next, we present two aggregation methods based on the characteristics of clients' local data. In Section 4.2, we assume a horizontal distribution of  $D_{\mathcal{I}}$ , that is, every client has access to the same set of interventions. Yet, assuming identical intervened covariates in interventional data is a naive assumption for real-world scenarios, where clients oftentimes hold interventional data on different features. Consequently, in Section 4.3, we propose a proximity-based belief aggregation applicable to clients with non-identical sets of intervened variables, i.e., vertical distribution of  $D_{\mathcal{I}}$ . It simulates a level of heterogeneity between clients in interventional data, since the underlying distributions vary across clients.

#### 4.1 Local discovery of prior beliefs

The goal in this stage is for each client to infer a belief about the global DAG. To this end, clients apply an LCDM to their local datasets,  $D^k$ . We expect the LCDM to produce and later incorporate prior knowledge about the structure, and favor this knowledge when uncertain about the existence of any  $X_i \rightarrow X_j \in E$ . We define clients' beliefs with matrices of the same dimensions as  $adj(G)$ .

**Definition 4.1 (Belief Matrix)** Let  $\psi \in \mathbb{R}^{N \times N}$  be the matrix with elements  $\psi_{ij}$ , where  $\psi_{ij}$  is the parameter of an independent Bernoulli distribution, i.e.,  $Ber(\psi_{ij}) \forall i, j$ . We call  $\psi$  the belief matrix, and each element,  $\psi_{ij}$ , corresponds to the existence probability of  $X_i \rightarrow X_j$ , i.e.,  $P(X_i \rightarrow X_j) \sim Ber(\mathcal{B}_{ij})$ . The matrix  $\psi$  results in an adjacency matrix by using an element-wise binary step function (threshold = 0.5).

We carefully pick neural LCDMs that learn similar belief matrices through continuous-optimization. For instance, ENCO [Lippe et al., 2021] uses  $\gamma, \theta \in \mathbb{R}^{N \times N}$  matrices to represent the existence and orientation of edges in a graph, respectively. This formulation is not unique to ENCO and other methods, such as SDI [Ke et al., 2019] and DCDI [Brouillard et al., 2020] use similar belief matrices. We mostly consider ENCO as clients' LCDM, owing to its efficient implementation and scalability.

The LCDM needs to consider the updated belief from the server into its local discovery process. We achieve this by directly initializing the LCDM belief matrices,  $\gamma, \theta$  in the case of ENCO, by sampling from Bernoulli distributions with  $\psi$  parameters, and enforcing this knowledge as a Lagrangian on LCDM's internal optimization loss function. More specifically, ENCO alternates between *distribution fitting* and *graph fitting* stages. Distribution fitting trains a neural network  $f_{\phi_i}$  to model  $X_i$ 's conditional data distribution,  $p(X_i | \mathbf{X}_{-i})$ , on observational data. Then, the graph fitting stage learns  $\gamma$  and  $\theta$  by minimizing

$$\mathcal{L} = \mathbb{E}_{\hat{I} \sim p_{I(I)}} \mathbb{E}_{\tilde{p}_{\hat{I}}(X)} \mathbb{E}_{p_{\gamma, \theta}(\zeta)} \left[ \sum_{i=1}^N \mathcal{L}_{\zeta}(X_i) \right] + \lambda_{sparse} \sum_{i=1}^N \sum_{j=1}^N \sigma(\gamma_{ij}) \cdot \sigma(\theta_{ij}), \quad (1)$$

where  $p_I(I)$  and  $\tilde{p}_{\hat{I}}(X)$  represent interventional data distribution and  $p_{\gamma, \theta}(\zeta)$  is the distribution over adjacency matrices with  $\zeta_{ij} \sim Ber(\sigma(\gamma_{ij})\sigma(\theta_{ij}))$ . Note that  $\sigma$  is the sigmoid function. Moreover,  $\mathcal{L}_{\zeta}(X_i) = -\log f_{\phi_i}(X_i; \zeta_{\cdot, i} \odot \mathbf{X}_{-i})$ , that is the negative log-likelihood estimate of the variable  $X_i$  with the distribution learned from observational data. The last term is for sparsity regularization<sup>1</sup>. We integrate an extra differentiable regularization term to consider the prior belief in Equation (1):

$$\tilde{\mathcal{L}} = \mathcal{L} + \lambda_{prior} \sum_{i=1}^N \sum_{j=1}^N -[\zeta_{ij} \log(\psi_{ij}) + (1 - \zeta_{ij}) \log(1 - \psi_{ij})], \quad (2)$$

where the log loss measures the agreement between the observed values in  $\zeta$  and the probabilities represented by  $\psi$ . Lower values of the log loss indicate a better agreement between  $\zeta$  and  $\psi$ , encouraging the optimizer to find solutions that align with the prior belief. Hence, the optimization process of LCDM is guided by the belief, especially when facing uncertainty about the existence of an arbitrary  $X_i \rightarrow X_j$ . Such uncertainties may arise when  $D_{\mathcal{I}}^k$  lacks interventional samples.

<sup>1</sup>Details of the optimization process and its tractability are provided in Lippe et al. [2021]

---

**Algorithm 1** FED-CD: federated causal discovery from observational and interventional data. We omit the description of basic functions for simplicity of presentation.

---

**Data:**  $D := \{D_{\mathcal{O}}, D_{\mathcal{I}}\}; \{C_1, \dots, C_K | K := \text{n\_clients} \in \mathbb{N}\}; T := \text{n\_rounds} \in \mathbb{N}$

**Return:**  $\tilde{G} :=$  estimation of the underlying causal structure (DAG)

```

for  $T$  iterations do ▷ federated rounds
  for  $k = 1$  to  $K$  do
     $\psi^k \leftarrow \text{local\_causal\_discovery\_method}(D^k, \psi)$  ▷ local learning (asynchronous and in parallel)
  end for
   $\psi \leftarrow \text{proximity\_based\_aggregation}(\psi, \{\psi^1, \dots, \psi^k\})$  ▷ model aggregation stage
end for
 $\tilde{G} \leftarrow \text{binary\_step}(\psi^*, \text{threshold} = 0.5)$  ▷ estimated causal DAG

function proximity_based_aggregation( $\psi, \{\psi^1, \dots, \psi^k\}$ )
   $\text{adj\_mat} \leftarrow \text{belief\_to\_adj}(\psi)$  ▷ latest structure from previous round's  $\psi$ 
  for  $X_i \rightarrow X_j$  in  $\text{edges}(\text{adj\_mat})$  do
    for  $k = 1$  to  $K$  do
      for  $X_s$  in  $X_{C_k}^{\mathcal{I}}$  do
         $\psi_{sp}^k, \dots, \psi_{ij}^k \leftarrow \text{get\_path\_beliefs}(X_s, X_i \rightarrow X_j)$  ▷ retrieves beliefs for all paths:
       $X_s \rightarrow X_p \rightarrow \dots \rightarrow X_i \rightarrow X_j$ 
       $r_{ij}^k \leftarrow \max(\psi_{sp}^k \cdot \dots \cdot \psi_{ij}^k \cdot m_s^k, r_{ij}^k)$  ▷ over paths like  $X_s \rightarrow \dots X_j \rightarrow X_i$ 
    end for
     $\hat{r}_{ij}^k = e^{\beta r_{ij}^k} / \sum_{k \in [K]} e^{\beta r_{ij}^k}$  ▷ reliability scores to probabilities
  end for
   $\psi_{ij}^* = \sum_{k \in [K]} \hat{r}_{ij}^k \psi_{ij}^k$  ▷ final aggregation
end for
return  $\psi^*$ 

```

---

## 4.2 Naive belief aggregation

In a naive scenario, we assume  $X_{\mathcal{I}}^k = X, \forall k \in \{1, \dots, K\}$ . Let  $\psi^k$  be the prior belief obtained by each client, after transmission of  $\psi^k$  to the server, the aggregated belief is calculated by a weighted average over  $\psi^k$  matrices through

$$\psi^* = \sum_k w_k \psi^k, \quad w_k = \frac{\text{size}(D^k)}{\text{size}(D)}, \quad \forall k \in \{1, \dots, K\}, \quad (3)$$

where  $\psi_{ij}^*$  is the aggregated belief. Because  $w_1 + w_2 + \dots + w_K = 1$ , each element of the weighted sum  $\psi_{ij}$  represents the parameter of a Bernoulli distribution. However, without access to same intervened covariates across clients' interventional dataset, this method fails to take client's expertise into account. For instance, a client with access to direct interventions on  $X_i$  is typically more confident about the edge probability of  $X_i \rightarrow X_j$  than a client without such knowledge.

## 4.3 Proximity-based belief aggregation

We know that  $D^k$ , contains interventions on the set of variables indicated by  $X_{C_k}^{\mathcal{I}}$ . After applying LCDM to the local data,  $\psi_{ij}^k$  is the posterior probability of  $X_i \rightarrow X_j$ 's existence, calculated by the client  $C_k$ . The question we are interested in is how to aggregate posteriors  $\psi_{ij}^k \forall k \in \{1, \dots, K\}$  while considering the clients' knowledge of interventions.

**Proposition 4.2** Consider  $X_i, X_j \in X$  to be two arbitrary variables in  $G$ . Then, for a client  $C_k$  admitting an intervened variable,  $X_s \in X_{\mathcal{I}}^k$ , the reliability of  $\psi_{ij}^k$ , denoted by  $r_{ij}^k \in [0, 1]$ , is higher if  $X_i \rightarrow X_j$  belongs to a path in  $G$  descending from  $X_s$ .

*Sketch of the proof.* Note that if the described path exists, then every variable  $X_i$  in the described path is a descendant of  $X_s$ . The proof is straightforward through causal factorization [Pearl, 2009],

$$P(X) = \prod_{i=1}^N P(X_i | \text{Pa}(X_i)) \Rightarrow P(X_i, X_j) = P(X_j | \text{Pa}(X_j)) \cdot P(X_i | \text{Pa}(X_i)). \quad (4)$$

Assuming an intervention on  $X_s$  and the truncated factorization formula (causal factorization with applied intervention [Pearl, 2009]), we write Equation (4) for  $X_i \rightarrow X_j$  as

$$P(X \setminus X_s \mid \text{do}(X_s = x)) = \prod_{i \mid X_i \neq X_s} P(X_i \mid \text{pa}_i) \Big|_x \quad (5)$$

$$\Rightarrow P(X_i, X_j \mid \text{do}(X_s = x)) = P(X_i \mid \text{pa}_i) \Big|_x P(X_j \mid \text{pa}_i) \Big|_x, \quad (6)$$

where it becomes clear that altering  $X_s$ 's distribution directly affects its descendants.

In order to find  $r_{ij}^k$  for each client, we inject hypothetical mass  $m_s^k$  to the node  $X_s$  and let the mass flow in the DAG without its magnitude being divided by the fan-out of each node. When passing through any edge  $X_q \rightarrow X_p$  on the way, the mass value is multiplied by  $\psi_{qp}$  where  $\psi_{qp}$  is the current aggregated belief in the network. The new mass then continues to flow in the graph in the same manner. For instance, the reliability score of the edge  $X_s \rightarrow X_p$  is  $\psi_{sp}^k m_s^k$ . The score becomes  $\psi_{sp}^k \psi_{pq}^k m_s^k$  for  $X_p \rightarrow X_q$ . Should different mass values reach the same node from multiple paths, we pick the maximum regardless of the source variables. After a sufficient number of steps, the mass flows through the entire DAG.

All clients perform the same process only once at each round, based on the latest aggregated belief,  $\psi$ . Let the mass passing through an edge be the reliability score for that edge. The process yields a set of reliability scores,  $\{r_{ij}^1, r_{ij}^2, \dots, r_{ij}^K\}$ , assigned to each edge  $X_i \rightarrow X_j$ . We cannot directly use  $r_{ij}^k$  values for aggregating the local beliefs  $\{\psi_{ij}^1, \psi_{ij}^2, \dots, \psi_{ij}^K\}$  as  $\sum_k r_{ij}^k \neq 1$ . To turn  $r_{ij}^k$  values into probabilities, we apply a softmax function and write the new aggregated belief as

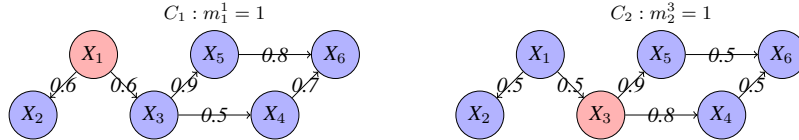
$$\psi_{ij}^* = \sum_{k \in [K]} \hat{r}_{ij}^k \psi_{ij}^k, \quad \hat{r}_{ij}^k = \frac{e^{\beta r_{ij}^k}}{\sum_{k \in [K]} e^{\beta r_{ij}^k}}, \quad \forall k \in \{1, \dots, K\}, \quad (7)$$

where  $\psi_{ij}^*$  is the aggregated belief and  $\beta > 0$  is the temperature parameter of the softmax function. The rate parameter  $\beta$  controls the sensitivity of the distribution of  $\hat{r}_{ij}^k$  to the difference of the reliability scores calculated by different clients. This procedure has the following parameters:

- $m_i^k, \forall i \in \{i \mid X_i \in \mathcal{X}_\mathcal{D}^k\}$ , the initial mass of  $C_k$ . We set this parameter proportionate to the number of interventional samples for  $X_i$  available in  $D^k$ .
- $\beta$ , the softmax temperature, optimized by a grid search over a reasonable range.

Algorithm 1 presents FED-CD and our novel proximity-based aggregation. We conclude this section by providing a toy example to illustrate the proposed belief aggregation.

**Example 4.2.1** Let's consider a 2-client setup.  $C_1$  has interventional samples on  $X_1$  (left), whereas  $C_2$  holds interventional data on  $X_3$  (right). We assume the clients have an equal number of samples,  $m_1^1 = m_2^3 = 1$ , and  $\beta = 2$  and  $\psi_{ij}$  acquired from last aggregation are written on the edges. Edges with  $\psi_{ij} < 0.5$  are omitted for simplicity of visualization.



The flow of mass for  $C_1$  and  $C_2$  yields:

$$r_{5,6}^1 = 0.6 \cdot 0.9 \cdot 0.8 \cdot m_1^1 = 0.432, \quad r_{5,6}^2 = 0.9 \cdot 0.5 \cdot m_3^2 = 0.540 \Rightarrow R_{5,6} = \{0.432, 0.540\}.$$

Then, the final reliability score of  $C_1$  and  $C_2$  for  $X_5 \rightarrow X_6$  is calculated by:

$$\hat{r}_{5,6}^1 = \frac{e^{(2 \times 0.432)}}{e^{(2 \times 0.432)} + e^{(2 \times 0.540)}} \approx 0.446, \quad \hat{r}_{5,6}^2 = \frac{e^{(2 \times 0.540)}}{e^{(2 \times 0.540)} + e^{(2 \times 0.432)}} \approx 0.554.$$

## 5 Experiments and Evaluation

We construct multiple federated setups to demonstrate the efficacy of FED-CD. We compare FED-CD results with the centralized approach, and the performance of a non-collaborating client. Next, we analyze naive averaging-based and

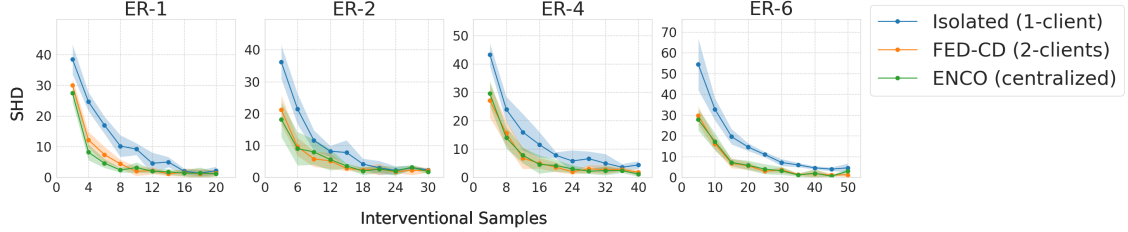


Figure 2: Our method is rigorously compared against a centralized approach and an isolated client, taking into account the size of the interventional data. In the centralized approach, the entire dataset is available, while in both FED-CD and the isolated client, each client is limited to only half of  $D$  distributed horizontally. This comprehensive comparison shows promising insights into the performance of FED-CD against a centralized approach.

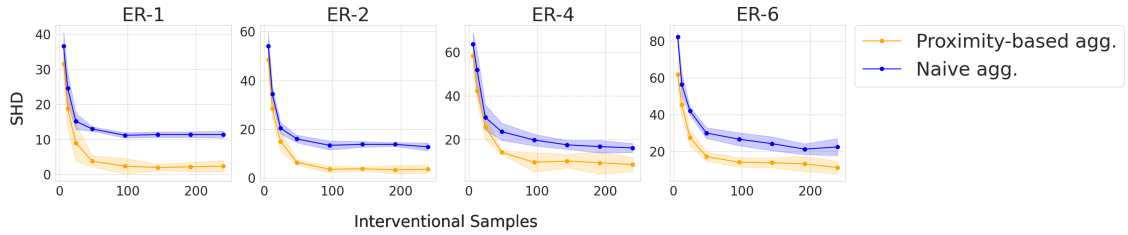


Figure 3: We apply the proximity-based and naive aggregation methods to vertically distributed  $D_{\mathcal{I}}$ . Each curve corresponds to a 5-client setup, where clients have access to disjoint and covering subsets of vertically distributed interventional dataset, i.e., local datasets contain interventional samples on only 4 out of 20 dataset features. The x-axis shows the size of  $D_{\mathcal{I}}$ .

proximity-based aggregation methods, especially elaborating on the shortcomings of the former facing vertical data distributions. We conclude by comparing FED-CD to methods in the literature on real-world and synthetic graphs, and analyzing its scalability.

## 5.1 Experimental setup

**DAGs** For synthetic data, we employ the random Erdős–Rényi (ER) model to pick experimental DAGs of size  $d = 20$ , where each edge is added with an independent pre-determined probability from the others [Erdős and Rényi, 2011]. Experiments are conducted for  $ER - n$  graphs where  $n \in \{1, 2, 4, 6\}$ . Based on the definition, the value of  $n.d$  is equal to the expected number of edges. For the real-world graphs in the last section, we turn to *bnlearn* package [Scutari, 2009], and pick Sachs [Sachs et al., 2005], Alarm [Beinlich et al., 1989], and Asia [Lauritzen and Spiegelhalter, 1988] DAGs from the dataset.

**Dataset** The global dataset,  $D$ , is generated based on the previously sampled DAGs, and by employing the synthetic sample generation mechanism similar to Ke et al. [2019]. The process utilizes randomly initialized neural networks – MLPs with two layers with categorical inputs – to model the ground-truth conditional distributions. We sample categorical data with 10 categories in different sizes for both interventional and observational sets. For all experiments, the observational data is horizontally distributed among clients. However, a client may receive interventional samples for all intervened variables (horizontal) or only a subset of those variables (vertical). Further details about the data generation process appear on Appendix B.

**Evaluation** We compare the outcome of each setup to the ground truth by calculating the Structural Hamming Distance (SHD) between the two. Note that the outcome for FED-CD is calculated by applying a binary step function (threshold = 0.5) to the most recent belief matrix. We then run each experiment for 20 random seeds, and report the average and confidence interval of the SHD results in all the plots and tables.

## 5.2 Horizontal data distribution

We start with a scenario where both  $D_{\mathcal{O}}$  and  $D_{\mathcal{I}}$  are split horizontally. Figure 2 presents multiple experiments with our method while employing the proximity-based aggregation (Section 4.3). The results demonstrate that two collaborative clients clearly outperform an isolated client. Moreover, it is evident that FED-CD can mostly discover a DAG with the

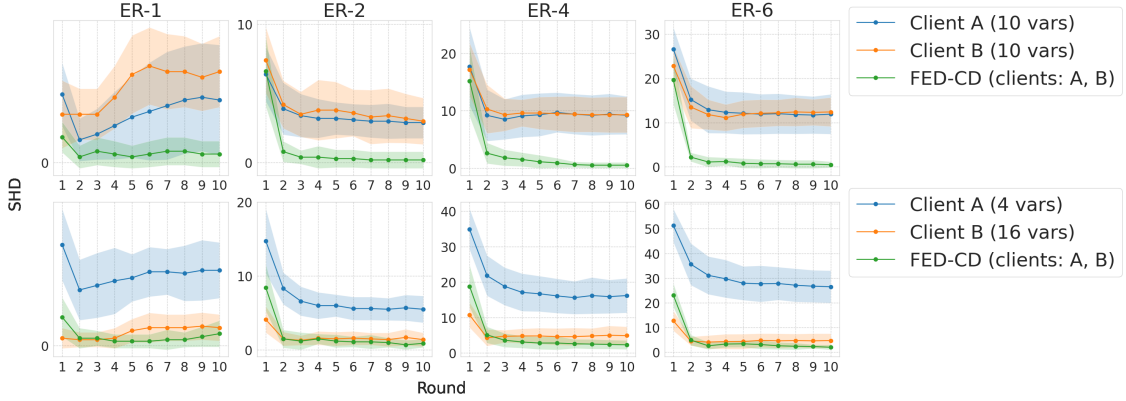


Figure 4: We compare three setups: non-collaborative clients A and B with access to vertical subsets of  $D_{\mathcal{I}}$ , and FED-CD where the same A and B clients now share their knowledge of the underlying structure. The results demonstrate the advantage of FED-CD in leveraging insights from both clients, highlighting its ability to harness diverse information, even from clients with access to fewer intervened covariates.

same precision as the centralized approach. Both comparisons suggest that the aggregation method is effectively and privately exchanging the knowledge of local dataset, causing improvement even in a simple horizontal distribution. Note that as the size of  $D_{\mathcal{I}}$  increases in Figure 2, the results of the isolated client come closer to FED-CD (and to the centralized approach), as each client now holds adequate samples to find the underlying DAG in a non-collaborative and centralized fashion.

### 5.3 Vertical distribution of interventional data

To highlight the critical role of interventional data in federated discovery, we turn to vertical distribution of  $D_{\mathcal{I}}$ , which limits clients' intervened variables to a subset of dataset features. From this angle, Figure 3 compares naive averaging-based aggregation method to the more sophisticated proximity-based aggregation. The results suggest that averaging-based approaches fail to discover the true structure, as they disregard clients' unique access to interventions.

We further showcase the capability of proximity-based aggregation through in Figure 4, where two isolated clients are compared against a 2-client federated setup, where these two clients start to collaborate through FED-CD. We observe a meaningful improvement as a result of collaboration. Moreover, Figure 4 illustrates that a client with access to the majority of interventional data still benefits from collaborating with the less significant client. This is justified as the second client holds key interventional samples critical for a more precise DAG discovery, and demonstrates the way our aggregation stage manages to reflect the opinion of such clients.

### 5.4 Performance with more collaborating clients

To assess the effect of increasing the number of clients, we performed two series of experiments in Figure 5. For the first setup, new clients join FED-CD by bringing their own local dataset. Therefore, the size of  $D_{\mathcal{I}}$  increases upon adding a new client, and more information becomes available in the network, while  $D^k$  have a fixed size. Then, we keep the  $\text{size}(D_{\mathcal{I}})$  constant, and then increase the number of clients. Each new client receives a share by joining the setup, leaving the others with fewer samples.

The results implicate that FED-CD experiences higher precision when clients with new information are added to the collaborative environment. Each client brings fresh samples, which in turn helps the aggregation stage to learn more accurate existence probabilities. However, even in the case of  $D_{\mathcal{I}}$ 's further division by adding new clients, FED-CD manages to perform consistently. Such results demonstrate that our aggregation technique is capable of efficiently gathering data from an increasing number of clients with less information, without having a detrimental effect on the overall efficiency. The only breaking point happens when clients are left with so few samples, that even the LCDM itself fails to converge to a local graph (see convergence conditions in Lippe et al. [2021]).

### 5.5 Baselines and generalization

We compare our setup against some well-known methods for DAG discovery by leveraging both interventional and observational data. From the methods listed in Guo et al. [2020], we pick GIES [Hauser and Bühlmann, 2012], IGSP

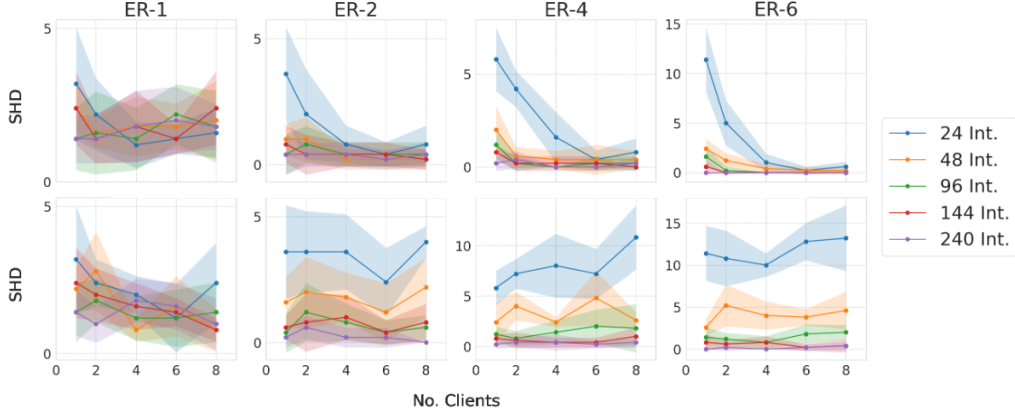


Figure 5: Effect of having more clients participate in FED-CD for different  $D_{\mathcal{I}}$  sizes. The discovered DAG is more accurate where  $\text{size}(D_{\mathcal{I}})$  increases with the addition of each new client (first row). FED-CD manages to sustain the knowledge when the fixed-size  $D_{\mathcal{I}}$  is further divided by the increase in number of clients (second row).

Table 1: Comparison between FED-CD and centralized baselines for synthetic and real-world graphs

DAG Type	ER-1	ER-2	ER-4	ER-6	Sachs	Alarm	Asia
GIES	$14.4 \pm 2.1$	$46.9 \pm 0.8$	$127.3 \pm 1.6$	$168.8 \pm 0.7$	$21.3 \pm 4.3$	$43.2 \pm 7.5$	$13.8 \pm 3.1$
IGSP	$11.8 \pm 2.8$	$43.7 \pm 0.7$	$118.5 \pm 0.4$	$152.8 \pm 0.1$	$14.4 \pm 3.4$	$25.1 \pm 1.4$	$12.6 \pm 2.7$
DCDI	$3.0 \pm 1.1$	$24.3 \pm 2.1$	$31.4 \pm 8.6$	$43.0 \pm 12.3$	$6.9 \pm 1.2$	$36.8 \pm 2.3$	$6.1 \pm 1.6$
ENCO	$1.9 \pm 0.1$	$4.3 \pm 0.1$	$5.7 \pm 0.2$	$7.8 \pm 0.3$	$0.5 \pm 0.4$	$13.8 \pm 2.5$	$1.9 \pm 0.1$
<b>FED-CD (2-clients)</b>	$2.6 \pm 0.6$	$3.9 \pm 0.4$	$4.1 \pm 0.1$	$5.5 \pm 0.3$	$0.9 \pm 0.3$	$14.2 \pm 0.8$	$1.5 \pm 0.6$
<b>FED-CD (4-clients)</b>	$2.3 \pm 0.4$	$3.3 \pm 0.7$	$4.6 \pm 0.6$	$5.7 \pm 0.4$	$0.8 \pm 0.5$	$13.9 \pm 3.1$	$1.7 \pm 0.4$

[Wang et al., 2017], and DCDI [Brouillard et al., 2020], apply them in a centralized manner to  $\{D_{\mathcal{O}}, D_{\mathcal{I}}\}$ , and report the results. The size of global datasets is the same for all methods, and is divided vertically between clients in FED-CD. The results indicate the capability of FED-CD in efficient knowledge aggregation, considering that each client has access to less information compared to centralized approaches, yet still the setup as a whole manages to yield precise discoveries. The last three graphs are adopted from *bnlearn* [Scutari, 2010].

## 6 Limitations and Future Work

**Limited data** We observed that in scenarios where each client has a limited local dataset, the DAG discovered by FED-CD is still better than individual estimates of clients but is not as promising as a centralized approach. Shortage in data samples could appear devastating when crossing a certain threshold. The threshold varies across different LCDMs and underlying data generation processes; therefore, future work could propose a generic method to yield this threshold.

**Computational complexity** Although running clients’ LCDM in parallel potentially reduces the overall computational time compared to a centralized approach, it can pose a higher computational load depending on the nature of the learning method. For instance, if the computational cost of the LCDM is linear regarding data and the overheads are negligible, then the computational load remains the same as a centralized approach. On the other hand, having a large overhead aside from dataset size leads to higher computational load compared to centralized approaches.

**Acyclicity** One must ensure that the adjacency matrix obtained after several rounds of aggregation is still a DAG. Pruning the adjacency matrix corresponding to the final estimation is one option. Yet, future work could integrate extra constraints in the aggregation process to ensure acyclicity.

## 7 Conclusion

We proposed a novel federated DAGs discovery from a distributed dataset to avoid sharing local and private samples to preserve clients’ privacy. Utilizing interventional data on top of observational samples, we can recover the underlying causal structure with high precision, and handle both vertical and horizontal distribution of interventional data without

direct exchange of information. Through comprehensive experiments, we showcased FED-CD’s scalability and performance compared to centralized methods. Most notably, we employ a naive aggregation approach to highlight the advantage of aggregation with attention to clients’ interventions. It is evident that FED-CD can be employed to effectively learn causal structures from decentralized data, while adhering to privacy concerns.

## 8 Reproducibility

To ensure the reproducibility of the results presented earlier in the paper, we have published the FED-CD’s source code <sup>2</sup>, accompanied by the essential reproducibility instructions that yield the plots depicted in the paper, provided in the main `README.mcl` file.

---

<sup>2</sup><https://www.github.com/aminabyaneh/fed-cd>

## References

- Ingo A Beinlich, Henri Jacques Suermont, R Martin Chavez, and Gregory F Cooper. The alarm monitoring system: A case study with two probabilistic inference techniques for belief networks. In *AIME 89*, pages 247–256. Springer, 1989.
- Philippe Brouillard, Sébastien Lachapelle, Alexandre Lacoste, Simon Lacoste-Julien, and Alexandre Drouin. Differentiable causal discovery from interventional data. *Advances in Neural Information Processing Systems*, 33: 21865–21877, 2020.
- Paul Erdős and Alfréd Rényi. On the evolution of random graphs. In *The structure and dynamics of networks*, pages 38–82. Princeton University Press, 2011.
- Erdun Gao, Junjia Chen, Li Shen, Tongliang Liu, Mingming Gong, and Howard Bondell. Federated causal discovery. *arXiv preprint arXiv:2112.03555*, 2021.
- Dorothy J Glancy. Privacy in autonomous vehicles. *Santa Clara L. Rev.*, 52:1171, 2012.
- Kui Xiang Gou, Gong Xiu Jun, and Zheng Zhao. Learning bayesian network structure from distributed homogeneous data. In *Eighth acis international conference on software engineering, artificial intelligence, networking, and parallel/distributed computing (snpc 2007)*, volume 3, pages 250–254. IEEE, 2007.
- Ruocheng Guo, Lu Cheng, Jundong Li, P Richard Hahn, and Huan Liu. A survey of learning causality with data: Problems and methods. *ACM Computing Surveys (CSUR)*, 53(4):1–37, 2020.
- Alain Hauser and Peter Bühlmann. Characterization and greedy learning of interventional markov equivalence classes of directed acyclic graphs. *The Journal of Machine Learning Research*, 13(1):2409–2464, 2012.
- Diviyan Kalainathan, Olivier Goudet, Isabelle Guyon, David Lopez-Paz, and Michèle Sebag. Structural agnostic modeling: Adversarial learning of causal graphs. *arXiv preprint arXiv:1803.04929*, 2018.
- Nan Rosemary Ke, Olexa Bilaniuk, Anirudh Goyal, Stefan Bauer, Hugo Larochelle, Bernhard Schölkopf, Michael C Mozer, Chris Pal, and Yoshua Bengio. Learning neural causal models from unknown interventions. *arXiv preprint arXiv:1910.01075*, 2019.
- Steffen L Lauritzen and David J Spiegelhalter. Local computations with probabilities on graphical structures and their application to expert systems. *Journal of the Royal Statistical Society: Series B (Methodological)*, 50(2):157–194, 1988.
- Tian Li, Anit Kumar Sahu, Ameet Talwalkar, and Virginia Smith. Federated learning: Challenges, methods, and future directions. *IEEE Signal Processing Magazine*, 37(3):50–60, 2020.
- Phillip Lippe, Taco Cohen, and Efstratios Gavves. Efficient neural causal discovery without acyclicity constraints. *arXiv preprint arXiv:2107.10483*, 2021.
- Osman Mian, David Kaltenpoth, Michael Kamp, and Jilles Vreeken. Nothing but regrets—privacy-preserving federated causal discovery. In *International Conference on Artificial Intelligence and Statistics*, pages 8263–8278. PMLR, 2023.
- Yongchan Na and Jihoon Yang. Distributed bayesian network structure learning. In *2010 IEEE International Symposium on Industrial Electronics*, pages 1607–1611. IEEE, 2010.
- Ignavier Ng and Kun Zhang. Towards federated bayesian network structure learning with continuous optimization. *arXiv preprint arXiv:2110.09356*, 2021.
- Nicolas Papernot, Patrick McDaniel, Arunesh Sinha, and Michael Wellman. Towards the science of security and privacy in machine learning. *arXiv preprint arXiv:1611.03814*, 2016.
- Judea Pearl. *Causality*. Cambridge university press, 2009.
- Karen Sachs, Omar Perez, Dana Pe'er, Douglas A Lauffenburger, and Garry P Nolan. Causal protein-signaling networks derived from multiparameter single-cell data. *Science*, 308(5721):523–529, 2005.
- Marco Scutari. Learning bayesian networks with the bnlearn r package. *arXiv preprint arXiv:0908.3817*, 2009.
- Marco Scutari. Learning bayesian networks with the bnlearn R package. *Journal of Statistical Software*, 35(3):1–22, 2010. doi: 10.18637/jss.v035.i03.
- Peter Spirtes. Introduction to causal inference. *Journal of Machine Learning Research*, 11(5), 2010.
- Peter Spirtes and Kun Zhang. Causal discovery and inference: concepts and recent methodological advances. In *Applied informatics*, volume 3, pages 1–28. SpringerOpen, 2016.
- Jan P Vandenbroucke, Alex Broadbent, and Neil Pearce. Causality and causal inference in epidemiology: the need for a pluralistic approach. *International journal of epidemiology*, 45(6):1776–1786, 2016.

- Matthew J Vowels, Necati Cihan Camgoz, and Richard Bowden. D'ya like dags? a survey on structure learning and causal discovery. *arXiv preprint arXiv:2103.02582*, 2021.
- Yuhao Wang, Liam Solus, Karren Dai Yang, and Caroline Uhler. Permutation-based causal inference algorithms with interventions. *arXiv preprint arXiv:1705.10220*, 2017.
- Karren Yang, Abigail Katcoff, and Caroline Uhler. Characterizing and learning equivalence classes of causal dags under interventions. In *International Conference on Machine Learning*, pages 5541–5550. PMLR, 2018.
- Qiaoling Ye, Arash A Amini, and Qing Zhou. Distributed learning of generalized linear causal networks. *arXiv preprint arXiv:2201.09194*, 2022.
- Yue Yu, Jie Chen, Tian Gao, and Mo Yu. Dag-gnn: Dag structure learning with graph neural networks. In *International Conference on Machine Learning*, pages 7154–7163. PMLR, 2019.
- Xun Zheng, Bryon Aragam, Pradeep Ravikumar, and Eric P Xing. Dags with no tears: Continuous optimization for structure learning. *arXiv preprint arXiv:1803.01422*, 2018.

## A Supporting Experiments

We present a comprehensive set of additional experiments with the FED-CD framework, aimed to put the proposed framework to test from a variety of angles.

### A.1 Performance per federated Rounds

Figure 6 experiments demonstrate the way FED-CD performs after each federated round. These experiments are conducted for two different dataset sizes, and are a special case of the plots shown in the main experiments. The plots indicate the framework’s improvement at the end of each round (aggregation step), and the resulting final convergence after a few rounds.

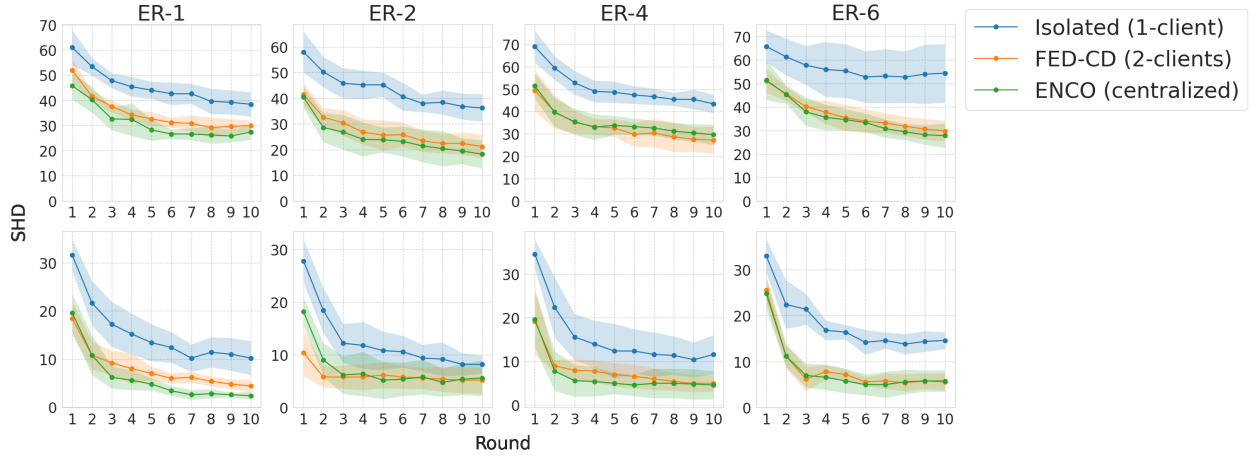


Figure 6: We provide a closer look into the gradual improvement at each federated round. Our method is compared against a centralized approach and an isolated client for two  $D_{\mathcal{I}}$  sizes: 4 (first row) and 20 (second row). The centralized approach has access to the entire dataset, while each client in FED-CD and the isolated client all have access to half of the dataset. The plots demonstrate that FED-CD is closely following a centralized approach at each federated round.

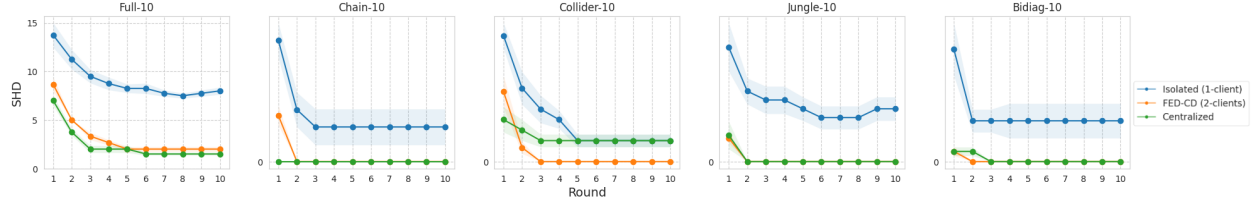


Figure 7: Evaluation of our approach when using SDI as the LCDM, instead of ENCO. We use structured graphs of size 10 here, and the improvement caused by the federated setup is still observable for all structured graph types. We need to reduce the graph size due to SDI’s computational time to achieve tractable experiments.

### A.2 Generalization to other LCDM candidates

We believe that other continuous-optimization based structure discovery methods can be employed as the LCDM in our approach if modifications explained in our Methodology are applicable. For instance, in Figure 7, we switch the LCDM from ENCO to SDI, a work on causal discovery investigated in our literature review. The results still indicate an improvement when employing a federated setup. Note that due to the heavy computational load of SDI, we are only experimenting on structured graphs with 10 nodes. For details about the underlying data generator graphs of these experiments, please refer to Appendix A.4.

### A.3 Investigating the average edge entropy

Consensus refers to the collective agreement among processes in a distributed setup to converge on a specific value, achieved through the voting of each process. Consensus plays a crucial role in federated learning. In this decentralized setting, achieving consensus ensures that all participating clients contribute to the model update in a synchronized manner, leading to a consistent and accurate global model. Consensus helps address the challenge of model divergence, where variations in local data and training conditions across clients can cause the models to drift apart. By reaching consensus, federated learning can mitigate the effects of data heterogeneity and ensure that the aggregated model represents a shared understanding of the data.

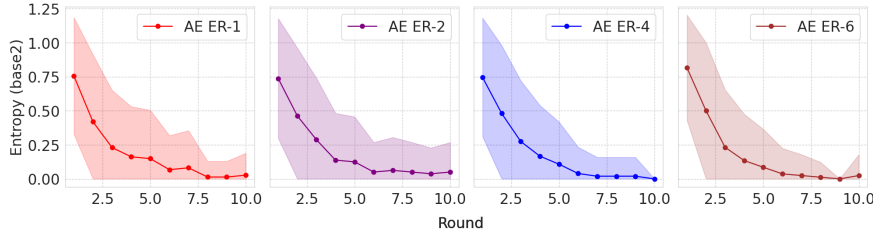


Figure 8: Average edge entropy for all the elements in the clients’ adjacency matrix for a 10-client federated setup is plotted here. The results reveal a substantial decrease in the values of edge entropy after each round, which serves as an empirical sign of convergence and indicates that the federated setup is progressing towards reaching a consensus.g clients over the rounds.

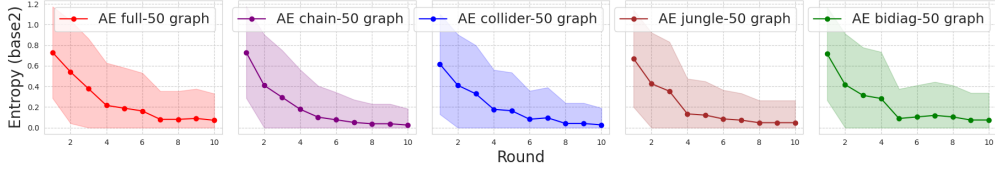


Figure 9: Average edge entropy for all the elements in the clients’ adjacency matrix for a 10-client federated setup plotted for structured graphs. The results reveal the same levels of decrease in the values of edge entropy after each round as Appendix A.3.

In our study, we assess the consensus achieved by calculating the average entropy (AE) for each edge. This measure is based on the information exchanged between clients and the server at the end of each round. The empirical results depicted in Appendix A.3 and Appendix A.3 showcase the dynamics of average entropy reduction across different causal graphs as the rounds progress. Remarkably, our proposed approach demonstrates the ability to attain consensus in most cases within 10 rounds, although in certain scenarios, we observe a substantial reduction in average entropy without reaching complete consensus. These findings highlight the effectiveness of our approach in reducing uncertainty and aligning the distributed processes towards a common understanding.

### A.4 Experiments on structured graphs

We conduct further experiments on a range of structured graphs to further evaluate FED-CD. These graphs include the *chain*, *bidiag*, *full*, *collider*, and *jungle* graphs. In the *bidiag* graphs, the probability of a node  $X_i$  being connected to its immediate parents  $X_{i-1}$  and  $X_{i-2}$  is defined as  $P(X_i = 1 | X_{i-1} = 1, X_{i-2} = 1)$ . Similarly, the *chain* graph represents a simplified version, where the probability of a node  $X_i$  being connected to its immediate parent  $X_{i-1}$  is defined as  $P(X_i = 1 | X_{i-1} = 1)$ . Collider graphs involve a specific node  $X$  having all other nodes as its parents, with the probability of a node  $X_i$  being connected to its parents being  $P(X_i = 1 | Pa(X_i))$ . The *full* graph represents the densest connected graph possible, where the probability of a node  $X_i$  being connected to all preceding nodes  $X_1, X_2, \dots, X_{i-1}$  is defined as  $P(X_i = 1 | X_1 = 1, X_2 = 1, \dots, X_{i-1} = 1)$ . Lastly, the *jungle* graph introduces a binary tree structure with additional connections to a node’s parent’s parent. These experiments provide valuable insights into how our approach performs under different graph configurations, capturing diverse causal relationships and their complexities.

Figure 10 and Figure 11 show FED-CD performing consistently on datasets generated by structured graphs. Note that all the graphs here have the same size 20 as the random graphs, and the datasets are produced with the same process of Lippe et al. [2021] and Ke et al. [2019] with the same sizes as the main paper. The next plot, Figure 12, depicts the experimental results for vertical distribution of  $D_{\mathcal{T}}$  where the underlying data generation process is built upon structured graphs, further verifying the results in the main paper.

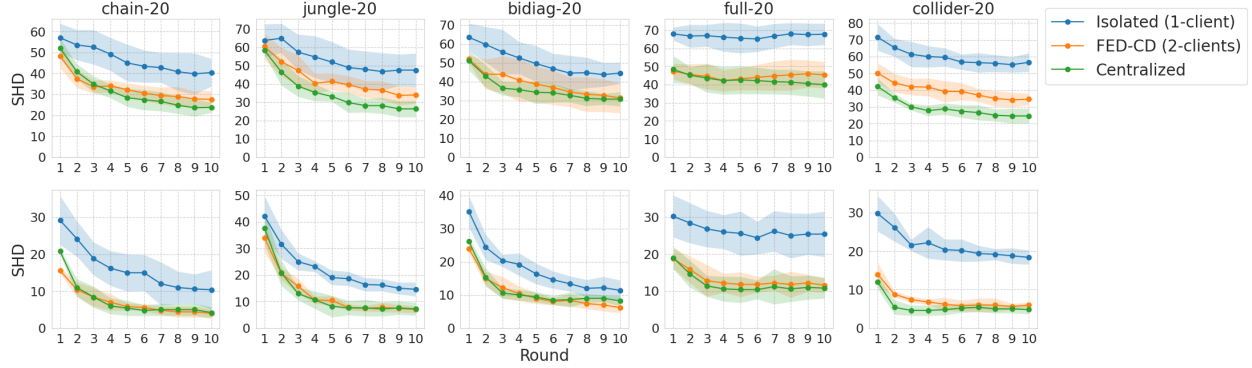


Figure 10: We provide a detailed analysis of the incremental improvement achieved in each federated round for *structured graphs*. Our method is compared against a centralized approach and an isolated client setting using two different sizes of  $D_{\mathcal{T}}$ : 4 (first row) and 20 (second row). In the centralized approach, the entire dataset is available, while in both FED-CD and the isolated client, each client has access to only half of the dataset. The plots clearly illustrate that FED-CD consistently tracks the performance of the centralized approach in every federated round.

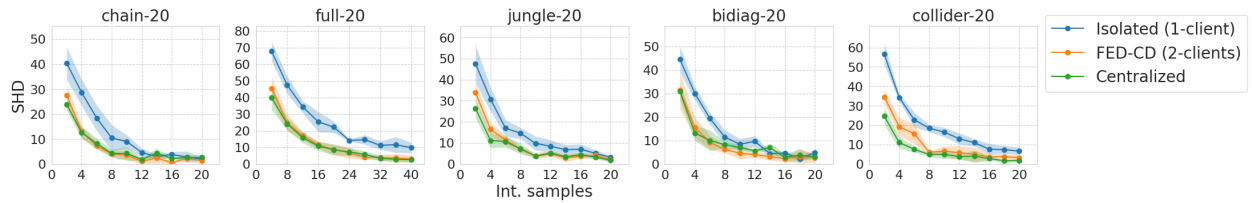


Figure 11: Our method is compared against a centralized approach and an isolated client based on the size of interventional data. The centralized approach has access to the entire dataset, while each client in FED-CD and the isolated client all have access to half of the dataset. The results of comparison to the centralized approach with structured graphs are aligned with that of the random ER graphs.

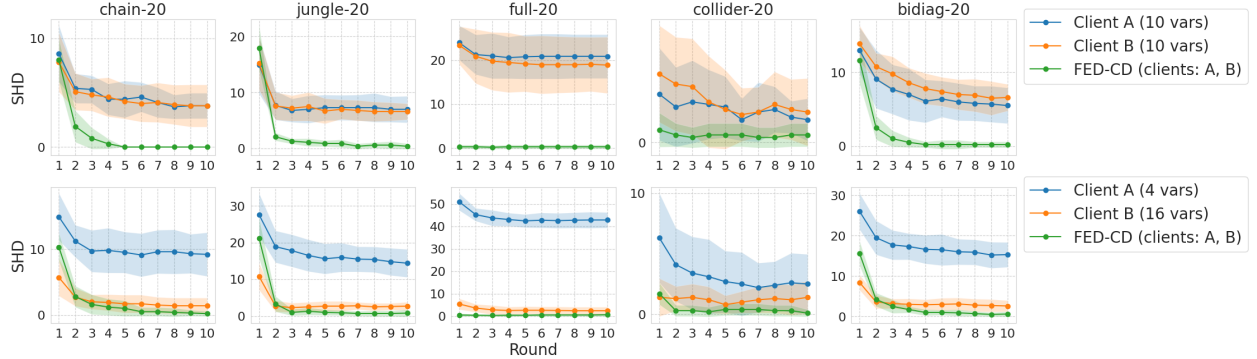


Figure 12: We compare three different setups with vertical distribution of  $D_{\mathcal{I}}$ , this time considering structured graphs. The setups are non-collaborative clients A and B with access to only a vertical subset of  $D_{\mathcal{I}}$ , and a federated setup where both clients collaborate through FED-CD. Evidently, FED-CD can take advantage of clients’ insight about the global structure, even from the less significant clients.

## B Experiment Setup and Details

### B.1 Dataset size and distribution

For the entire experiments, aside from the baselining table, we use  $10k$  observational samples as  $D_{\mathcal{O}}$  and  $2k$  samples for  $D_{\mathcal{I}}$ . For the baselining, however, we increase the size of  $D_{\mathcal{O}}$ ,  $D_{\mathcal{I}}$  to  $25k$  and  $5k$  to make the experiments compatible with other methods such as IGSP. These numbers correspond to the size of  $D$ , that is, the global dataset yet to be distributed among several clients. For example, in a 2-client setup, each client typically gets half of the observational data. Depending on the vertical or horizontal split of the interventional data, a client might get access to samples from all or part of dataset features.

### B.2 Graph and dataset generation

We adhere to the random Erdős–Rényi [Erdős and Rényi, 2011] model to generate experimental DAGs of size  $d = 20$ . Erdős–Rényi graphs, named after mathematicians Paul Erdős and Alfréd Rényi, are a type of random graph model that provides a simple and fundamental framework for studying random network structures. These graphs are characterized by their random and independent edge formation. Each edge is added with an independent pre-determined probability from the others, and is modeled by  $G(d = 20, p)$ . Hence, each edge is included in the graph with probability  $p$ . The probability for generating a graph that has  $d$  nodes and  $n$  edges is  $p^n(1 - p)^{\binom{d}{2} - n}$ .

Our experiments are conducted for  $ER - n$  graphs where  $n \in \{1, 2, 4, 6\}$ . The value of  $m = n.d$  (where  $n$  is the parameter in  $ER - n$ ) is equal to the expected number of edges. For example, as  $d = 20$  throughout the experiments, an  $ER - 2$  DAG has an expected number of  $m = 40$  edges. Further, to determine the orientation of the edges, we assume the causal ordering of  $(X_i, X_j)$  to be oriented  $X_i \rightarrow X_j$  if  $i < j$ , otherwise  $X_j \rightarrow X_i$ .

Same as Lippe et al. [2021] and Ke et al. [2019], we employ categorical variables of 10 categories each. The process utilizes randomly initialized neural networks – MLPs with two layers with categorical inputs – to model the ground-truth conditional distributions. For instance, when a variable  $X_i$  has  $M$  parents,  $M$  embedding vectors are stacked and passed as an input. The hidden size of the layers is 48, and their architecture uses a LeakyReLU activation functions between layers and a softmax activation to find a distribution for the output. More information about the process could be found in the appendix of Lippe et al. [2021].